Nanoscale

Accepted Manuscript

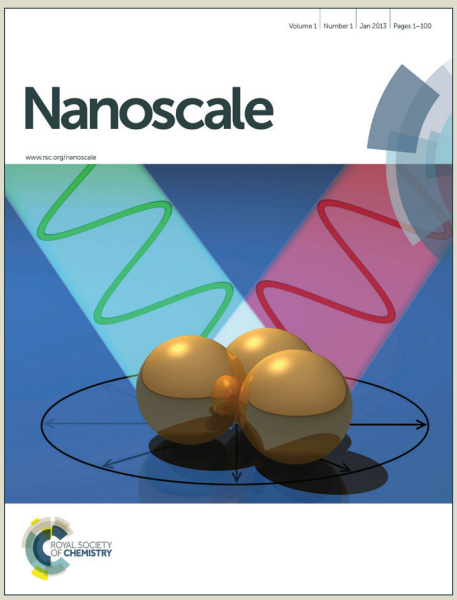

ROYAL SOCIETY OF CHEMISTRY

www.rsc.org/nanoscale

Nanoscale

RSCPublishing

ARTICLE

Hyaluronan-decorated polymer nanoparticles targeting CD44 receptor for the combined photo/chemo-therapy of cancer†

Cite this: DOI: 10.1039/x0xx00000x

Received 00th January 2015,
Accepted 00th January 2015

DOI: 10.1039/x0xx00000x

www.rsc.org/

Sara Maiolino,[a,#] Francesca Moret,[b,#] Claudia Conte,[a] Aurore Fraix,[c] Pasquale Tirino,[d] Francesca Ungaro,[a] Salvatore Sortino,[c] Elena Reddi[b] and Fabiana Quaglia [a,*]

In the attempt to develop novel concepts in the design of targeted nanoparticles for combination therapy of cancer, here we propose CD44-targeted hyaluronan-decorated double-coated nanoparticles (dcNPs) delivering the lipophilic chemotherapeutic Docetaxel (DTX) and an anionic porphyrine ($TPPS_4$). dcNPs were based on electrostatic interactions between a negative DTX-loaded nanoscaffold of poly(lactide-co-glycolide), a polycationic shell of polyethylenimine entangling negatively-charged $TPPS_4$ and finally decorated with hyaluronan (HA) to promote internalization through CD44 receptor-mediated endocytosis. DTX/$TPPS_4$-dcNPs, prepared through layer-by-layer deposition, showed hydrodynamic diameter around 180 nm, negative zeta potential and efficient loading of both DTX and $TPPS_4$. DTX/$TPPS_4$-dcNPs were freeze-dried with trehalose giving a powder that could be easily dispersed in different media. Excellent stability of dcNPs in specific salt- and protein-containing media was found. Spectroscopic behavior of DTX/$TPPS_4$-dcNPs demonstrated a face-to-face arrangement of the $TPPS_4$ units in non-photoresponsive H-type aggregates accounting for an extensive aggregation of the porphyrin embedded in the shell. Experiments in MDA-MB231 cells overexpressing CD44 receptor demonstrated a 9.4-fold increase of intracellular level of $TPPS_4$ delivered from dcNPs as compared to free $TPPS_4$. Light-induced death was increased tremendously in cells that had been treated with the combination of $TPPS_4$ and DTX delivered through dcNPs as compared with free drugs, presumably due to efficient uptake and co-localization inside cells. In perspective, the strategy proposed here to target synergistic drug combinations through HA-decorated nanoparticles seems very attractive to improve specificity and efficacy of a cancer treatment.

Introduction

Combination chemotherapy has long been adopted as the standard of care against many cancer types. It is generally recognized that through the proper drug combination, the treatment can promote synergistic actions, improve target selectivity, and prevent the development of cancer drug resistance.[1-3] This approach has been found promising when Photodynamic Therapy (PDT) has been combined to conventional chemotherapy in the management of several cancer types.[4-7] In PDT a photosensitizer (PS), after irradiation at specific wavelength, causes mainly the formation of the cytotoxic species singlet oxygen ($^1O_2$) which reacts with tissue components, leading to cell death through the initiation of apoptosis and necrosis.[8] Indeed acting by different mechanisms, cytotoxic drugs can act in concert with PS for tumor killing, achieving potentiated therapeutic outcome through an anticancer synergistic effect.

Entrapment of multiple therapeutic agents in a nanocarrier offers an unprecedented opportunity to devise a better scheme for precise and controlled delivery of multiple therapeutic agents in the same area of the body and at predefined

†Electronic Supplementary Information (ESI) available: Synthetic and experimental procedures. See DOI: 10.1039/b000000x/

#Contributed equally to the work
[a]Drug Delivery Laboratory, Department of Pharmacy, University of Napoli Federico II, Via Domenico Montesano 49, 80131, Napoli, Italy
Email: quaglia@unina.it
[b]Department of Biology, University of Padova, via U. Bassi 58/b, 35121 Padova, Italy
[c]Laboratory of Photochemistry, Department of Drug Science, Viale Andrea Doria 6, 95125, Catania, Italy
[d]Department of Chemistry Paolo Corradini, University of Napoli Federico II, Via Cintia, 80126 Napoli, Italy,

extra/intracellular level.[9-14] As compared to other nanocarriers, polymer-based nanoparticles (NPs) offer a great prospect in this area since they can be designed to target a solid tumor, to incorporate drugs with different solubility and to deliver them at finely tuned rates.[15] By exploiting the presence of dysfunctional endothelium of tumor capillary wall and the absence of effective lymphatic drainage in solid tumors, biomimetic and long –circulating NPs can partly extravasate from the blood circulation and reach solid tumor interstitium.[16,17] This mechanism referred as Enhanced Permeability and Retention (EPR) effect is the main determinant in passive targeting while surface modification with structural motifs able to specifically recognize peculiar elements of tumors have been explored to further ameliorate drug specificity and effective drug accumulation in tumors/cancer cells.[18-20] Furthermore, timing of drug release (temporal control of drug availability at target site) can be finely tuned. From a therapeutic standpoint, drug release rate is of key importance to drive administration scheme (number of administrations, frequency) as well as to optimize cell response. In particular, sustained release of some chemotherapeutics from Polymer NPs are gaining overwhelming interest since they are expected not only to amplify cell response and extend activity to hypoxic zones of certain tumors but also to improve drug activity resembling a metronomic therapy (subactive doses for longer time frames).[21]

Despite of their great potential, there have been very few attempts in developing tumor-targeted nanosystems for the co-delivery of PS and anticancer drugs.[22-26] A challenging task in the development of polymeric NPs for combination therapy resides in the design of systems carrying drugs with a different solubility. Core-shell architecture represents an effective way to serve this purpose and to attain multiple functionalities on a nanoscopic length scale. In one of the possible configurations, a polymeric hydrophobic core (template), generally carrying a lipophilic chemotherapeutic agent, is surrounded by one or more than one polymeric hydrophilic layers that entraps an interacting drug and provides a functional interface with biological environment. As core-forming polymers, poly(lactide-co-glycolide)s (PLGA) are excellent candidates to form NPs with sustained delivery features. By varying polymer molecular weight and crystallinity, facile control on both encapsulation efficiency and biodegradation rate, and in turn on drug delivery rate, are attained.[27] Amid shell-forming hydrophilic polymers, hyaluronan (HA) is emerging for its activity as biological response modifiers in cancer.[28,29] HA is widely employed in cancer to direct a drug or a NP to tumor tissues due to its ability to recognize HA receptors (CD44, RHAMN) which are overexpressed in different cancer cell lines.[28,30] Receptor-mediated endocytosis facilitates drug transport inside the cells and contributes to improve cytotoxicity.[31] It has been recently demonstrated that targeting a receptor such as CD44, which can undergo recycling between cell surface and endosomes/lysosomes and mediate transcytosis, can also promote tumor penetration of NPs in a tumor tissue.[32]

Here, we develop CD44-targeted double-coated NPs (dcNPs) for the combined conventional and photodynamic therapy of cancer delivering the lipophilic taxane Docetaxel (DTX) and the negatively-charged PS Tetrasodium-Meso-tetra(4-sufonatophenyl)porphyrine ($TPPS_4$). dcNPs based on a DTX-PLGA core template and decorated with HA via electrostatic interactions with polyethyleneimine (PEI) as positively-charged $TPPS_4$-containing bridging polymer were produced and fully characterized for colloidal properties, photochemical behavior and phototoxicity in cancer cell lines overexpressing the CD44 receptor.

Materials and methods

Chemicals

Docetaxel (DTX, MW=807.88) was purchased from LC laboratories (USA). Poly (D,L-lactide-co-glycolide) (PLGA) (50:50 Resomer RG 502H inherent viscosity 0.16-0.24 dl/g) was purchased from Boehringer Ingelheim (Ingelheim, Germany). Tetrasodium-Meso-tetra(4-sufonatophenyl)porphyrine ($TPPS_4$, MW=1239.1) was purchased from Frontier Scentific. Rhodamine B (RHO), trehalose, polyethyleneimine (PEI, MW ~ 25 kDa branched), poloxamer 188 (pluronic® F68), copper (II) sulphate, hexadecyltrimethyl-ammonium bromide, sodium acetate, sodium chloride, sodium hydroxide, glacial acetic acid and trifluoracetic acid (TFA) were purchased from Sigma-Aldrich. Acetonitrile and acetone were purchased from Carlo Erba Reagenti (Milan, Italy). DMEM and Fetal Bovine Serum (FBS) were purchased from Gibco life technologies. Hyaluronan (HA, MW <10 kDa) was a kind gift of Magaldi Life S.r.l. Ultrapure water was used throughout the study. N-(4,4-difluoro-5,7-dimethyl-4-bora-3a,4a-diaza-indacene-3-pentanoyl)sphingosine (BODIPY® FL C5-ceramide) and LysoTracker® Green DND-26 were from Molecular Probes (Life Technologies, Milan, Italy). The CellTiter96® Aqueous One Solution Cell proliferation Assay (MTS) was from Promega Co (Madison, USA).

Preparation of double-coated nanoparticles (dcNPs)

dcNPs loaded with DTX, $TPPS_4$ or DTX/$TPPS_4$ (DTX-dcNPs, $TPPS_4$-dcNPs, DTX/$TPPS_4$-dcNPs) were prepared by a layer-by-layer deposition method. Briefly, DTX-loaded PLGA NPs were prepared by solvent diffusion of an organic phase (10 mg of PLGA and 0.5 mg of DTX in 2 mL of acetone) in an aqueous phase (4 mL of water with Pluronic F68 0.1%). After solvent evaporation, the sample was splitted in 4 Eppendorf® tubes, centrifuged (5000 x g for 15 min, Mikro 20, Zentrifugen) and the pellets dispersed in 1 mL water. NPs in each tube were coated first with 125 µL of a PEI water solution (1 mg/mL) and centrifuged (2800 x g for 10 min). The supernatant was discarded and the pellet dispersed in 1 mL water. Thereafter, the sample was added with 25 µL of a $TPPS_4$ water solution (0.2 mg/mL) followed by 100 µL of a HA water solution (1 mg/mL). The interval between each addition was kept constant at 15 min. dcNPs were freeze-dried for 24 h after addition of trehalose (30 mg/Eppendorf® tube) as cryoprotectant and kept at 4 °C. Recovery yield of production process was evaluated on an aliquot of DTX/$TPPS_4$-dcNPs nanoparticles (without cryoprotectant) by weighting the solid residue after freeze-

drying. Results are expressed as the ratio of the actual NP weight to the theoretical polymer weight × 100.

Characterization of dcNPs

Size, surface charge and morphology. Hydrodynamic diameter, polydispersity index (PI) and zeta potential of NPs after each preparation step were determined on a Zetasizer Nano Z (Malvern Instruments Ltd., UK). Results are reported as mean of three separate measurements of three different batches (n=9) ± SD. NP morphology was examined by Transmission Electron Microscopy (CM 12 Philips, Eindhoven, The Netherlands) staining samples with a 2% w/v phosphotungstic acid solution..

DTX and $TPPS_4$ actual loading. DTX loading inside DTX/$TPPS_4$-dcNPs was assessed by placing 0.5 mg of freeze-dried NPs (without cryoprotectant) in 500 µL of DCM and overnight stirring until a film was formed at bottom of the vial. Thereafter, 500 µL of water and 500 µL of acetonitrile were added and the sample was filtered through a 0.45 µm filter (RC, Chemtek, Italy). DTX was analyzed by HPLC on a Shimadzu (Japan) apparatus equipped with a LC-10ADvp pump, a SIL-10ADvp autoinjector, a SPD-10Avp UV–Vis detector and a C-R6 integrator. The analysis was performed on a Supelco 5 µm, C18 column (250 × 4.6 mm, Å). The mobile phase was a 55:45 (v/v) mixture of water with TFA 0.1 % and acetonitrile pumped at a flow rate of 1 mL/min. The UV detector was set at 227 nm. A calibration curve for DTX in ethanol was constructed in the concentration range 0.980–19.6 µg/mL. The limits of quantification (LOQ) and detection (LOD) were 1.29 and 0.39 µg/mL, respectively. DTX recovery in the presence of unloaded NPs was around 100%.
$TPPS_4$ loading inside DTX/$TPPS_4$-loaded dcNPs was evaluated in the supernatant by UV after NP centrifugation at 13000 x g for 15 min. A calibration curve was constructed at 413 nm (UV 1800, Shimadzu, Japan) in the $TPPS_4$ concentration range 0.05-5 µg/mL.

PEI and HA dosage. PEI amount in DTX/$TPPS_4$-dcNPs was quantified by a colorimetric method developed previously.[33] Freeze-dried NPs (0.5 mg, without cryoprotectant) were treated with 1 mL of 1 M NaOH and stirred overnight. The sample (0.5 mL) was diluted with 0.5 mL of 1 M acetic acid. The resulting solution (0.5 mL) was added to 1 mL of a 0.1 M acetate buffer at pH 5.4 and complexed with 0.25 mL of a copper (II) sulphate water solution (0.1% w/v). The absorbance value of each solution was recorded at 281 nm. A calibration curve was constructed in the PEI concentration range 15–380 µg/mL.
To evaluate the extent of HA adsorption onto NPs, DTX/$TPPS_4$-dcNPs (0.5 mg) were centrifuged at 13000 x g for 15 min and the supernatant was freeze-dried. The solid residue was then dissolved in 1 mL of 0.2 M acetate buffer (0.2 M sodium acetate and 0.15 M sodium chloride) at pH 6. Thereafter, 2 mL of hexadecyltrimethyl-ammonium bromide reagent (2 g sodium hydroxide, 1 g hexadecyltrimethyl-ammonium bromide in 100 mL water) were added and the sample was analyzed at 350 nm. A calibration curve was constructed in the HA concentration range 10–200 µg/mL.

DTX and $TPPS_4$ release. In vitro release of DTX and $TPPS_4$ was performed on 30.5 mg of freeze-dried powder (corresponding to 0.5 mg of NPs) dispersed in 1 mL DMEM FBS+ 10% at 37°C. At predetermined time intervals, the sample was centrifuged 13000 x g (15 min). $TPPS_4$ release as assessed in the supernatant by spectrophotometry at wavelength of 422 nm. A $TPPS_4$ calibration curve in the range 0.2-4 µg/mL was constructed in the release medium.
DTX release was assessed by HPLC as reported in 2.2.2 after treating 1 mL of medium with acetonitrile (1 mL) to precipitate proteins and final centrifugation at 13000 x g (15 min). Results are expressed as % release overtime ± SD of three experiments.

Spectroscopic and photochemical experiments

Absorption and emission. UV/Vis absorption and fluorescence spectra were recorded with a thermostated HP-8452 diode array spectrophotometer and Fluorolog-2 (Model, F-111) spectrofluorimeter respectively. All measurements were performed in a thermostated quartz cell (1 cm path length, 3 mL capacity). Fluorescence spectra were corrected by the different fraction of absorbed photons by the different samples at the excitation wavelength.

Laser flash photolysis. All samples were excited with the second harmonic of Nd–YAG Continuum Surelite II–10 laser (532 nm, 6 ns FWHM), using quartz cells with a path length of 1.0 cm. The excited solutions were analyzed with a Luzchem Research mLFP–111 apparatus with an orthogonal pump/probe configuration. The probe source was a ceramic xenon lamp coupled to quartz fiber-optic cables. The laser pulse and the mLFP–111 system were synchronized by a Tektronix TDS 3032 digitizer, operating in pre-trigger mode. The signals from a compact Hamamatsu photomultiplier were initially captured by the digitizer and then transferred to a personal computer, controlled by Luzchem Research software operating in the National Instruments LabView 5.1 environment. The solutions were deoxygenated by bubbling with a vigorous and constant flux of pure nitrogen (previously saturated with solvent). In all of these experiments, the solutions were renewed after each laser shot (in a flow cell of 1 cm optical path), to prevent probable photodegradation processes. The sample temperature was 295 ± 2 K. The energy of the laser pulse, measured at each shot with a SPHD25 Scientech pyroelectric meter, was ca. 10 mJ/pulse.

Cell studies

Cells. Human breast cancer cell lines MDA-MB231 and MCF-7 were purchased from American Type Tissue Culture Collection (ATCC, Rockville, Maryland). The cells were grown in DMEM with Glutamax™ supplemented with 10% heat-inactivated fetal bovine serum (FBS), 1 mM sodium pyruvate, 100 U/mL streptomycin and 100 µg/mL penicillin G (Life Technologies, Milan, Italy), and maintained at 37 °C in a humidified atmosphere containing 5% CO_2.

Uptake studies. Flow cytometry experiments were carried out to investigate the expression level of CD44 receptor and its involvement in the internalization of fluorescent dcNPs labeled with RHO (RHO-dcNPs) in MDA-MB231 and MCF-7 and to measure the uptake of $TPPS_4$ and $TPPS_4$-dcNPs in MDA-MB231 cells. RHO-dcNPs were prepared as described in 2.1 by incorporating a 20% w/w of PLGA covalently linked to RHO in

the PLGA core (supplementary material S1). RHO-dcNPs were used in place of $TPPS_4$-dcNPs for studying CD44-mediated internalization of NPs to avoid any misleading result generated by $TPPS_4$ release in the cell external medium.

The level of CD44 expression in MDA-MB231 and MCF-7 cells was measured by staining the cells with a FITC-conjugated anti-CD44 antibody (Abcam, Cambridge, UK). To study the role of CD44 in the uptake of RHO-dcNPs, 4 x 10^4 cells were grown in 24-well plates for 24 h and incubated for 2 h with 50 µg/mL of NPs diluted in medium added with 3% FBS. Some samples were pre-incubated for 1 h with 10 mg/mL free HA (Sigma-Aldrich, St. Louis, USA) in order to saturate CD44 receptors before NP addition and incubation (competition experiments). At the end of the incubation time, the cells were washed twice with Versene™, detached from the plates with trypsin, that was neutralized by the addition of FBS. Cells were centrifuged and resuspended in Versene™ before measuring RHO fluorescence using a BD FACSCanto™ II flow cytometer (Becton Dickinson, San Jose, USA). The blue laser at 488 nm was used for excitation and the PE channel (564-606 nm) was selected for the detection of RHO fluorescence. For each sample 105 events were acquired and analyzed with the FACSDiva software.

For $TPPS_4$ and $TPPS_4$-dcNPs uptake, cells were seeded and handled as described above and incubated for 24 h with increasing concentrations of PS in medium added with 3% FBS. For the detection of $TPPS_4$ fluorescence wavelengths longer than 670 nm were selected.

Cytotoxicity assay. Viability of MDA-MB231 cells incubated with free $TPPS_4$, free DTX, $TPPS_4$-dcNPs, DTX-dc NPs, DTX/$TPPS_4$-dcNPs and empty dcNPs in the absence of light was measured with the MTS assay. This assay measures cell metabolic activity (dehydrogenase enzyme activity) and therefore is largely used to evaluate cell viability and proliferation. Cells (5 x 10^3) were seeded in 96-well plates (24 h of growth) and then incubated with the various formulations

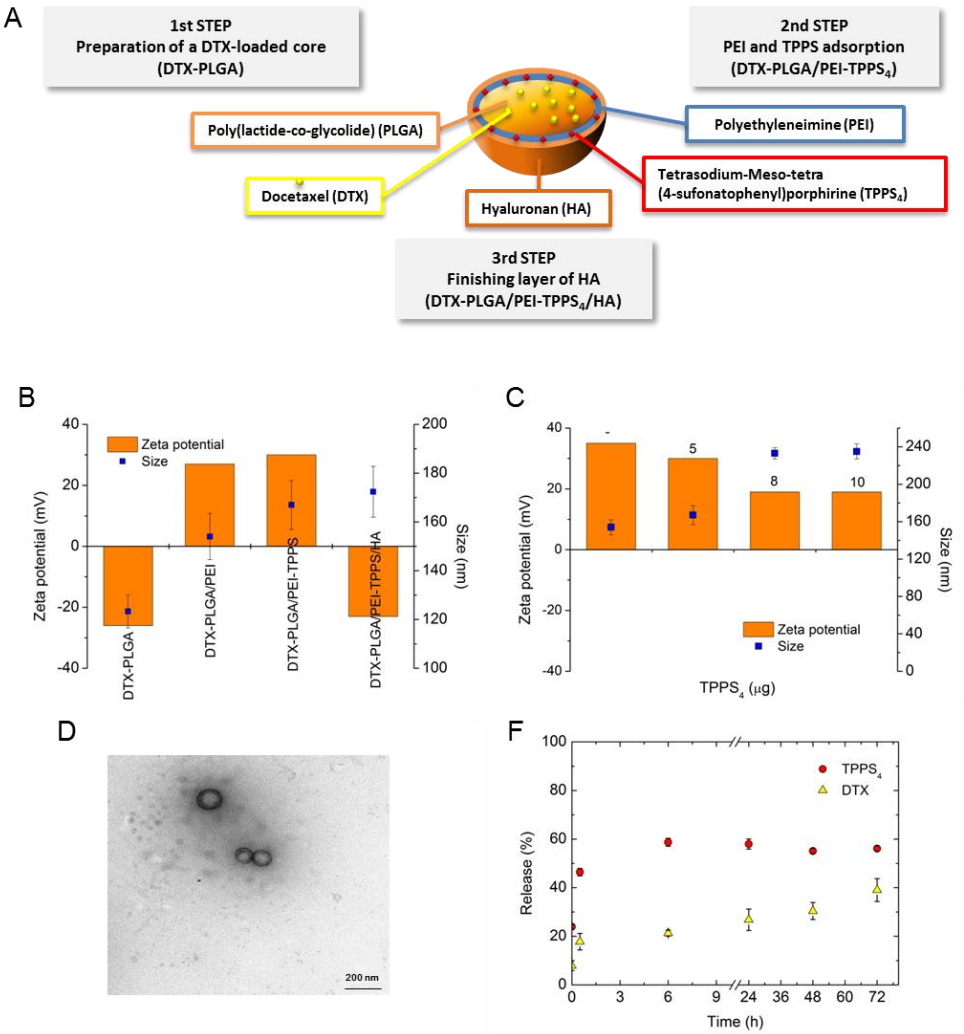

Fig. 1 Structure and properties of dcNPs. A) Schematic representation of the structure of DTX/$TPPS_4$-dcNPs and steps for their preparation; B) evolution of zeta potential and size during NP layering; C) effect of different concentration of $TPPS_4$ on zeta potential and size; C) TEM image of DTX/ $TPPS_4$ dcNPs; D) Release profile o$TPPS_4$ and DTX from dcNPs in DMEM FBS+ at 37 °C.

diluted in medium added with 3% FBS. Cell viability was measured at the end of incubation time (24, 48, 72 h) as well as after additional 24 h in which the cells were kept in drug-free medium (24 + 24 h). For MTS assay the culture medium was replaced with 100 µL of serum-free medium and 20 µL of CellTiter 96® Reagent and the wells were incubated for 1 h at 37 ◦C. The absorbance at 492 nm was measured with a Multiskan Go (Thermo Fischer Scientific, Waltham, USA) plate reader and the viability of treated cells was expressed as percentage of the absorbance of control cells that was taken as 100% viability.

In vitro photo-toxicity. MDA-MB231 cells (5 x 10^3) were grown for 24 h and incubated for further 24 h with free $TPPS_4$, combination of free $TPPS_4$ and free DTX, $TPPS_4$-dcNPs, DTX/$TPPS_4$-dcNPs and empty dcNPs in the dark. After incubation with the drugs, the cells were washed twice with PBS with Ca^{2+} and Mg^{2+}, and irradiated in PBS with 8 J cm^{-2} of blue light (390-460 nm, fluence rate 11 mW cm-2) from a UV 236 lamp (Waldmann Eclairage SA, Germany). Immediately after irradiation the cells were brought back to the incubator after replacement of PBS with fresh medium. Cell viability was measured with the MTS test after additional 24 h.

Statistical analysis. The Primer software for biostatistics (McGraw-Hill, Columbus, USA) was used for statistical analysis of the data. The data are expressed as means ± standard deviations (SD) of at least 3 independent experiments. The difference between groups were evaluated with the Student's t-test and considered significant for $p < 0.05$.

Results

Preparation and characterization of double-coated nanoparticles

Double-coated nanoparticles (dcNPs) made of a negatively-charged PLGA core loaded with the lipophilic drug DTX, a positively-charged bridging layer of PEI embedding the water-soluble $TPPS_4$ and a negatively-charged HA coating were produced through electrostatically-driven layer-by-layer assembly (Fig. 1A). Layering was followed through size and zeta potential measurements. DTX-PLGA NPs have a negative charge due to the presence of carboxylic end groups and adsorb firstly the positively charged PEI and then the negatively charged $TPPS_4$ through electrostatic interactions. Amount of PEI added strongly affected dispersibility of NPs after the washing step (data not shown). During layering, the size of NPs progressively increased up to around 50 nm and zeta potential is reversed after each polymer layer deposition step (Fig. 1B).
$TPPS_4$ adsorption onto PEI layer covering DTX-PLGA core did not alter size and zeta potential of NPs up to a $TPPS_4$ amount of 5 µg (Fig. 1C). At this concentration, $TPPS_4$ was quantitatively adsorbed onto NPs as demonstrated by the fact that the supernatant does not give any appreciable ABS at maximum absorption wavelength of $TPPS_4$. Final dcNPs show a hydrodynamic diameter below 180 nm and a net negative zeta potential. Actual loading of DTX and $TPPS_4$ in the final formulation is 0.95 ± 0.5 and 0.97 ± 0.2 mg per 100 mg of dcNPs, respectively. Amount of PEI and HA adsorbed onto final formulation is 7.94 ± 2.1 and 12.2 ± 0.8 mg per 100 mg of dcNPs, respectively. DTX/$TPPS_4$-dcNPs can be freeze-dried with trehalose to produce a powder that can be easily redispersed in water giving the original NP properties in term of size, PI and zeta potential as well as absorption properties (see ESI, Fig. S2). Morphology of DTX/TPPS4-dcNPs was evaluated by Transmission Electron Microscopy (Fig. 1D). The images revealed that discrete spherical NPs were formed with no aggregation. Coating layer on NPs could be also discriminated from the PLGA core. Release profile of DTX and $TPPS_4$ from DTX/$TPPS_4$-dcNPs was assessed in DMEM FBS+ at 37 °C and evaluated up to 72 h to simulate conditions occurring in cell studies. dcNPs display slow DTX release while 20% of $TPPS_4$ is immediately released probably due to its high solubility in the medium (Fig. 1E). DTX release is much slower than that of $TPPS_4$ as expected from their different lipophilicity.

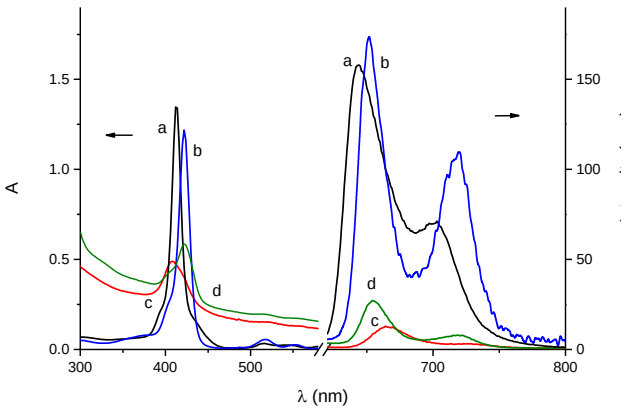

Fig. 2 Absorption (left) and fluorescence emission (right) spectra of TPPS4 and DTX/TPPS4-dcNPs in water (a,c) and in DMEM FBS+ (b,d). λex= 530 nm.

Spectroscopic and photochemical experiments

Fig. 2 shows the absorption and fluorescence emission spectra of DTX/$TPPS_4$-dcNPs and, for comparison, those of free $TPPS_4$ in water and in DMEM FBS+.
In water solution, the free $TPPS_4$ shows a sharp Soret band with a maximum centered at 413 nm (a, left) and a double band fluorescence emission with maxima at 640 and 700 nm (a, right), respectively. These spectral features are typical for the monomeric form of $TPPS_4$.[34] In the presence of DMEM, the Soret absorption is always narrow but undergoes a slight hypochromism and significant red-shift (b, left). Besides, a red-shift was also observed in the fluorescence emission but the fluorescence quantum yield was only slightly affected by DMEM (b, right). This spectroscopic scenario excellently reflects that reported for the same porphyrin in the presence of micellar systems[34] and is consistent with the presence of $TPPS_4$ mainly as a monomer in DMEM FBS+.
The spectroscopic properties of $TPPS_4$ are profoundly affected when it is loaded within the dcNPs. In particular, a broadening of the Soret band accompanied by a dramatic hypocromic effects and blue-shift of ca. 6 nm was observed (c, left). Besides, the fluorescence was significantly suppressed and the

emission bands were both red-shifted of ca. 16 nm (c, right). This spectroscopic behavior is typical for a face-to-face arrangement of the $TPPS_4$ units in non-photoresponsive H-type aggregates[34,35] and thus accounts for an extensive aggregation of the porphyrin in the dcNPs. However, the low but not negligible fluorescence emission observed, suggests a slight deviation from the strict parallel arrangement of the dipole moments of $TPPS_4$ units.[36]

The whole DTX/$TPPS_4$-dcNPs are quite stable in the presence of DMEM FBS+. In fact, the absorption spectrum (d, left) shows the Soret band shifted in two components with maxima at ca. 408 and 420 nm, respectively. While the former component is related to the H-types aggregates of $TPPS_4$ in the dcNPs, the latter indicates that a small fraction of $TPPS_4$ (ca. 20 %) undergoes displacement and is released in its monomeric form in DMEM medium. Accordingly the fluorescence spectrum (d, right) showed a slight revival with the emission maxima corresponding well to those observed for the free $TPPS_4$ in the same medium (see spectrum b, right). This scenario is well confirmed by the behavior of the lowest triplet state of $TPPS_4$. This excited state is the key transient intermediate for the photosensitization of $^1O_2$ and its effective generation is thus crucial for the photodynamic action.[37,38]

Laser flash photolysis with nanosecond time-resolution is a powerful tool for obtaining spectroscopic and kinetic features of excited triplets of porphyrins since these transient species exhibit very intense absorptions in the visible region and possess lifetimes falling in the microsecond time scale.[39] Fig. 3 shows that the transient spectra observed 0.1 μs after laser excitation of $TPPS_4$ free and DTX/$TPPS_4$-dcNPs dispersed in water and in DMEM FBS+, respectively. Excitation of aqueous solutions of free $TPPS_4$ resulted in the formation of a transient absorption with a maximum at ca. 440 nm and a bleaching due to the Soret ground-state absorption (Fig. 3, spectrum a). This species decays mono-exponentially with a lifetime of ca. 20 μs (Fig. 4A), and can be safely attributed to the lowest excited triplet state of the $TPPS_4$.

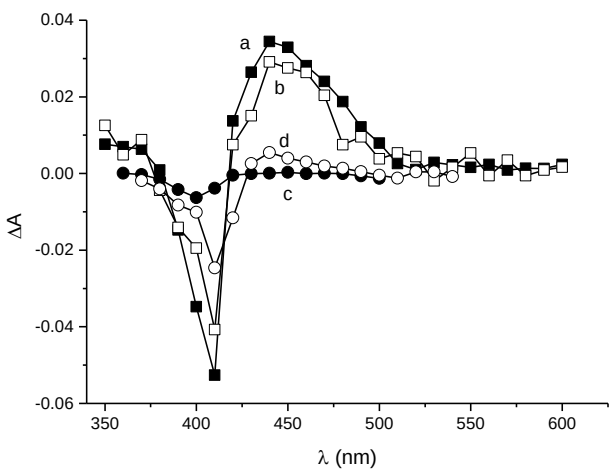

Fig. 3 Transient absorption spectra observed 0.1 μs after 532 nm laser excitation (E_{532} ~ 10 mJ/ pulse) of N_2-saturated solutions of $TPPS_4$ in water (a) and DMEM FBS+ (b) and DTX/$TPPS_4$-dcNPs in water (c) and DMEM FBS+ (d). Each point is the average of five laser shots.

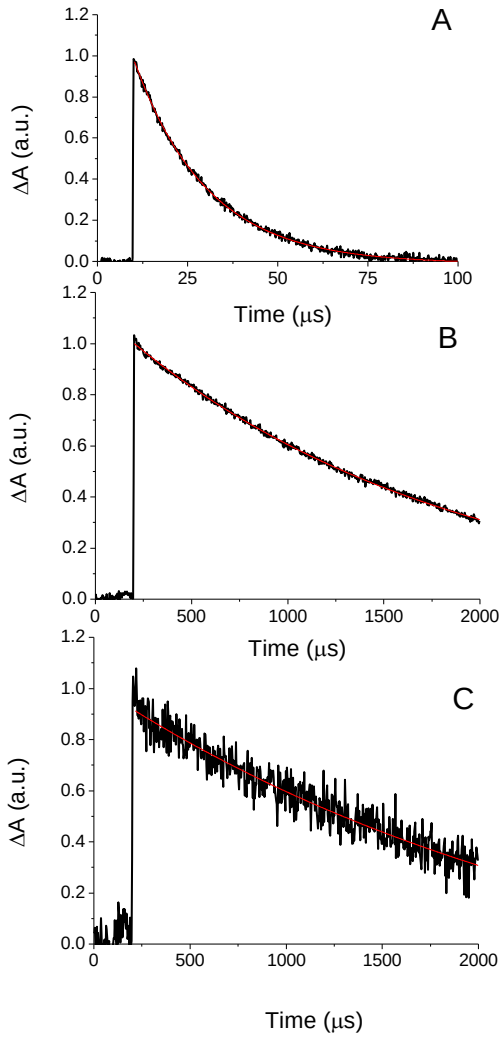

Fig. 4 Normalized decay traces monitored at 440 nm and the related first-order fittings, observed upon 532 nm laser excitation (E532 ~ 10 mJ/ pulse) of N2-saturated of TPPS4 in water (A) and DMEM FBS+ (B) and DTX/TPPS-dcNPs in DMEM FBS+ (C). Each decay trace is the average of five laser shots.

The triplet state of $TPPS_4$ is also effectively populated in the presence of DMEM FBS+ (Fig. 3, spectrum b) but its lifetime was much longer being ca. 1.5 ms (Fig. 4B). In contrast, no significant transient signal was observed for DTX/$TPPS_4$-dcNPs in water (Fig. 3, spectrum c) according to the assembling of the porphyrin in the form of non-photoresponsive H-type aggregates within dcNPs. In the presence of DMEM FBS+, DTX/$TPPS_4$-dcNPs exhibited a weak revival of the triplet signal. The appearance of this signal can be due to the displacement of the $TPPS_4$ from the nanoparticles and its release in DMEM medium under as photoactive monomeric form. The triplet decay observed in these conditions (Fig. 4C) was in fact virtually the same to that observed for the free $TPPS_4$ under the very same experimental conditions (see, Fig. 4B).

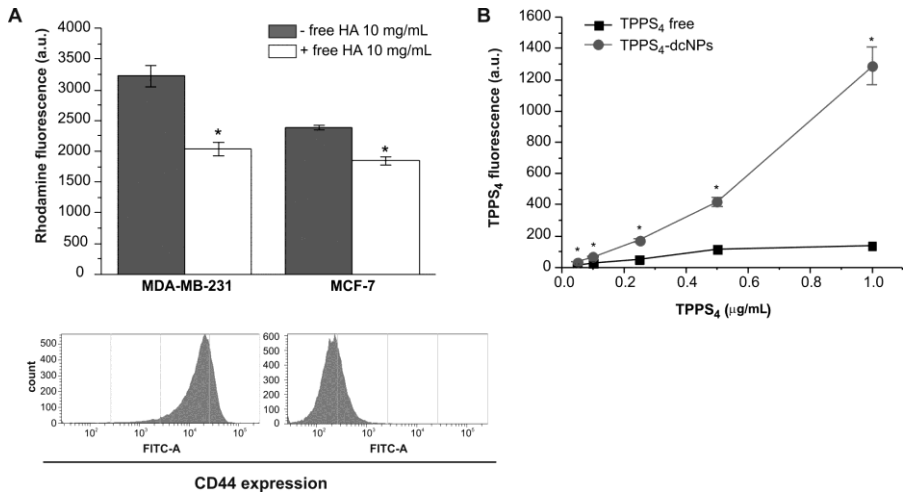

Fig. 5 Uptake of RHO-dcNPs and TPPS4-dcNPs. A) Uptake of RHO-dcNPs (50 μg/mL) in MDA-MB-231 (high CD44 expression) and MCF-7 (low CD44 expression) cells after 2 h incubation at 37 °C in medium with or without 10 mg/mL free HA. * p<0.001, with respect to the sample not incubated with free HA (Student's t test). B) Concentration-dependent uptake of free TPPS4 and TPPS4-dcNPs in MDA-MB-231 cells after 24 h incubation at 37 °C. * p<0.001, with respect to TPPS4 free (Student's t test).

CD44-mediated cell uptake of dcNPs

The involvement of CD44 receptor in the uptake of HA-coated NPs was studied measuring the uptake of RHO-dcNPs in MDA-MB-231 and MCF-7 cells exhibiting high and low CD44 expression, respectively. As shown in Fig. 5 A, RHO-dcNPs were taken up by both cells lines but as expected, the uptake was significantly higher in MDA-MB-231 with respect to MCF-7 cells. The active role of CD44 in mediating the uptake of a large dcNPs fraction was further confirmed with the competition experiments in which the cells were pre-incubated with an excess of free HA in order to saturate the receptors. The reduction of NP uptake caused by free HA was significant in both cell lines but it was more important in MDA-MB-231 than MCF-7 cells (37% vs 23%) showing a clear dependence on the expression levels of CD44. Given the more important role of CD44 in MDA-MB-231, with respect to MCF-7 cells, the first were selected for our uptake and cytotoxicity studies on $TPPS_4$ and DTX delivered by dcNPs. The uptake of $TPPS_4$, delivered to the cells in the free form or incorporated in $TPPS_4$-dcNPs was measured by flow cytometry after 24 h of cell incubation (Fig. 5 B). Delivery through dcNPs significantly increased the uptake of the PS at all tested concentrations and, at the highest concentration of 1 μg/mL, the uptake of $TPPS_4$-dcNPs was about 9.4-folds that of free $TPPS_4$. Confocal microscopy analysis revealed that while free $TPPS_4$ was localized both in lysosomes and Golgi apparatus, $TPPS_4$-dcNPs localized exclusively in lysosomes (see ESI, Fig. S3).

Cytotoxicity of dcNPs

The cytotoxicity of DTX toward MDA-MB-231 cells was determined for the free and DTX-dcNP formulation by incubating the cells up to 72 h. The cell viability was reduced at low drug concentrations but reached a plateau at approx. 0.1

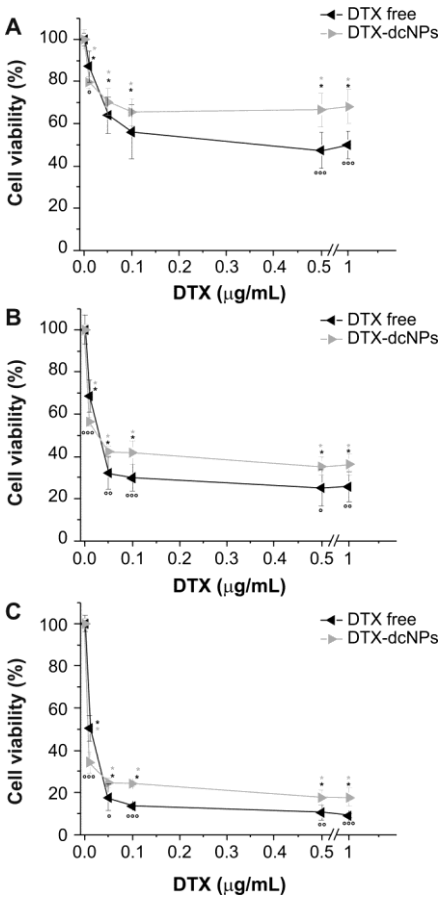

Fig. 6. Cell viability of MDA-MB-231 cells exposed to increasing concentrations of free DTX or DTX-dcNPs for 24 (A), 48 (B), 72 h (C). * p<0.001, with respect to control (Student's t test). ° p<0.05, °° p<0.01, °°°p<0.001, with respect to DTX-dcNPs (Student's t test).

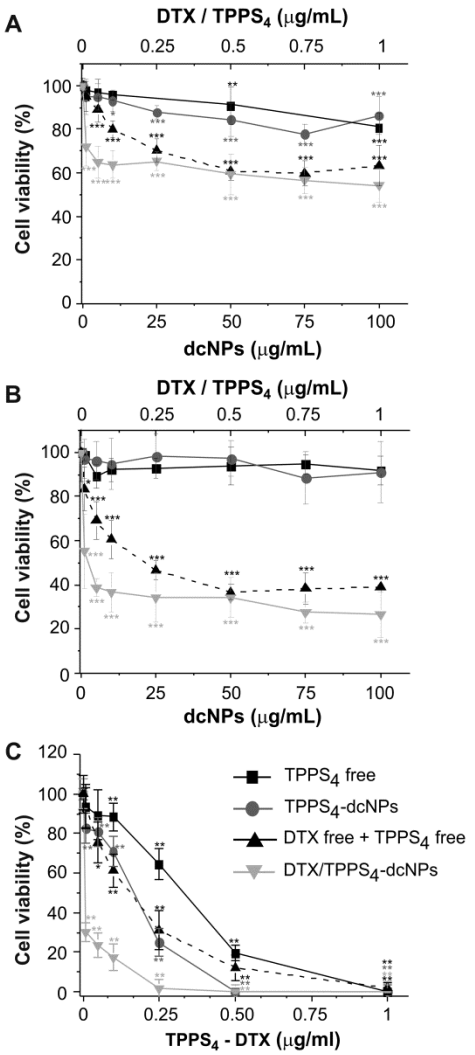

Fig. 7 Viability of MDA-MB-231 cells exposed in the dark to drugs free or loaded in dcNPs for 24 h (A) or 24 + 24 h (B). *p<0.05, **p<0.01, ***p<0.001, with respect to control (Student's t test). In C) the cells were irradiated with 8 J/cm^2 of blue light after 24 h of exposure to the drugs and viability was measured 24 h post-irradiation. *p<0.01, **p<0.001, with respect to control (Student's t test).

μg/mL DTX (Fig. 6). The residual cell viability in the plateau region decreased prolonging the time of treatment for both formulations. DTX delivered by dcNPs was significantly more cytotoxic at very low concentrations (e.g. 0.01 μg/mL) while, increasing the dose, free DTX resulted more effective in inducing cell death. DTX induced cell death by causing an arrest in the phase G2M of the cell cycle as already shown for taxanes (see ESI, Fig. S4). However, our cell cycle analyses carried out after 24 h of treatment with DTX showed that DTX-dcNPs were significantly more efficient in inducing the block in G2M, especially at doses as low as 0.01 μg/mL. At this concentration, free DTX did not cause appreciable alterations of cell distribution in the various phases of the cycle while DTX-dcNPs increased the percentage of cells in S and G2M phases. This result is consistent with higher loss of cell viability measured at low concentrations of DTX-dcNPs with respect to free DXT.

The toxicity of free $TPPS_4$ and $TPPS_4$-dcNPs was measured in the absence of light after 24 h or 24 + 24 h of cell incubation for concentrations up to 1 μg/mL. Both PS formulations were scarcely cytotoxic toward MDA-MB-231 cells, with no more than 20% of cell mortality at 1 μg/mL $TPPS_4$ (Fig. 7 A, B). Prolonging the incubation up to 72 h did not increase cytotoxicity (data not shown).

MDA-MB-231 cells treated for 24 h with DTX/TPPS4-dcNPs showed a decrease of viability similar to that induced by DTX-dcNPs ($p>0.05$, Bonferroni test) (Fig. 6 A), indicating that in the dark cytotoxicity is mainly due to DTX. The combination of the two drugs in their free form caused a decrease of cell viability similar to that of DTX/$TPPS_4$-dcNPs at concentrations higher than 0.25 μg/mL while at lower concentrations the combination of the free drugs was significantly less cytotoxic than DTX/$TPPS_4$-dcNPs (Fig. 7 A, B).

No effects on cell viability was observed incubating the cells with empty dcNPs up to 72 h with NP concentrations up to 100 μg/mL (see ESI, Fig. S5).

Cytotoxicity was also measured in cells incubated for 24 h with the various $TPPS_4$ formulations and then exposed to 8 J cm-2 of blue light. As shown in Fig. 7 C, $TPPS_4$ delivered through dcNPs was significantly more phototoxic than the free form, with an IC50 of 0.17 and 0.33 μg/mL PS, respectively. As expected, light-induced death was increased in cells that had been treated with the combination of $TPPS_4$ and DTX in dcNPs (IC50 0.008 μg/mL PS). Interestingly, the decrease of cell viability after irradiation induced by DTX/$TPPS_4$-dcNPs was significantly higher than that induced by the combination of the free drugs (IC_{50} 0.16 μg/mL PS). Control experiments showed that empty dcNPs and irradiation with blue light did not affect the viability of MDA-MB-231 cells (see ESI S6).

Discussion

The main goal of this work was to develop biodegradable core-shell dcNPs for combined delivery of photo- and chemo-therapeutics in cancer cells overexpressing CD44 receptor. To this end, we exploited the strong electrostatic interactions between different and ad-hoc chosen, functional blocks. A biodegradable PLGA nanoscaffold, carrying the hydrophobic chemotherapeutic DTX, was surrounded by a HA/PEI shell, entangling the hydrophilic PDT agent $TPPS_4$ to give the complete nanoassembly. The rationale behind this logical design is summarized in the following: (1) HA is expected to be exposed at the dcNPs periphery, ensuring the active targeting to cancer cells; (2) the hydrophobic DTX and the hydrophilic $TPPS_4$ are located in different compartments of the dcNPs (i.e., the core and the shell); such a large separation distance rules out any intermolecular communication between the photoexcited PDT agent and DTX (i.e. photoinduced electron transfer); (3) the cationic PEI is expected to encourage the extensive aggregation of the PDT agent at the dcNPs shell; as a consequence, $TPPS_4$ is expected to be nonfluorescent and unable to photosensitize $^1O_2$ until it is released from the dcNPs in its monomeric form.

From a formulation standpoint, the amount of $TPPS_4$ loaded on PEI-coated NPs had an impact on size, which suggests that upon $TPPS_4$ adsorption some rearrangement of PEI chains due

to altered negative to positive charge ratio could occur. Freeze-drying of dcNPs was feasible by using trehalose as cryoprotectant. After dispersion of the powder in water, spherical, non-aggregated DTX/$TPPS_4$-dcNPs with unaltered hydrodynamic diameter and zeta potential were obtained. Size below 200 nm and negative surface perfectly fit the biological requirements for injectable nanoparticles.[40] As generally found for polyelectrolyte systems, the size of DTX/$TPPS_4$-dcNPs was very dependent on the presence of salts and proteins. As a general trend, dcNPs were prone to size and zeta potential (less negative) increase in the presence of salts. For polyelectrolyte NPs where HA is adsorbed onto chitosan cross-linked NPs, a tendency to NP shrunk is observed due to an increased osmotic pressure of the medium which decreases NP swelling.[31] Indeed, we observed an opposite trend for DTX/$TPPS_4$-dcNPs which could be contributed by formation of weaker electrostatic interactions between PEI and HA as well as formation of a looser PEI/HA network. The different arrangement of PEI/HA chains can explain also the burst release of monomeric $TPPS_4$ (around 20%). Finally, a further increase of dcNP size in DMEM FBS+ could be attributed by protein adsorption onto NP surface possibly due to higher extent of exposition of positively-charged PEI to the medium. It is expected that PEI positive amino groups are prone to protein interaction as demonstrated for PEI or different types of nanoparticles.[41,42]

Since targeting ability of HA-coated NPs is strongly related to the morphology of the surface HA and in turn its mode of exposition to CD44 receptor[43,44], we preliminarily evaluated if dcNPs could be internalized in cancer cells. dcNPs bound CD44 receptor and were internalized by the cells with an efficiency that depended on the level of CD44 expression; as a matter of fact the uptake of Rho-dcNPs was significantly higher in MDA-MB-231 cells that exhibited a high CD44 expression than MCF-7 cells. The active role of CD44 was confirmed by the higher inhibition of dcNP uptake in MDA-MB-231 with respect to MCF-7 cells when an excess of free HA was added to the cell medium before and during incubation with NPs. However, the uptake of dcNPs was not completely abolished by free HA suggesting that a fraction of NPs, that is similar in the low- and high-expressing CD44 cells, was internalized via a CD44-independent endocytosis.

Both $TPPS_4$ and DTX entrapped in dcNPs could benefit of the CD44-mediated internalization of their carrier by increasing selective uptake and cytotoxicity in CD44 over-expressing cancer cells. $TPPS_4$ is an efficient hydrophilic photosensitizer of $^1O_2$ in solutions.[45] Nevertheless it remains a poor photosensiting agent in vitro and in vivo due to its inability to enter and to be retained inside the cells[46,47] at adequate concentrations able to produce efficient cell photoinactivation. Its incorporation into dcNPs greatly enhances its uptake in MDA-MB-231 cells and consequently increases the efficiency of light-induced cell mortality. $TPPS_4$ loaded in dcNPs at 1 μg/mL was clearly detected in the lysosomes of the cells while intracellular fluorescence of free $TPPS_4$ was much less intense and was localized both in lysosomes and Golgi apparatus. It is worth mentioning that previous studies on cellular localization of free $TPPS_4$ were carried out at a concentration of 75 μg/mL for gaining a fluorescence signal sufficient to detect a precise lysosomal localization of the porphyrin in the cells.[48] In line with our observations, Varchi et al.[49] reported undetectable fluorescence in HepG2 cells incubated with free $TPPS_4$ (20 μg/mL) while $TPPS_4$ delivered to cells in polymethylmethacrylate NPs showed a high intracellular fluorescence. Consistent with these observations our flow cytometry measurements showed higher uptake of $TPPS_4$ in dcNPs with respect to the free form; at 1 μg/mL the uptake in NPs was increased by approximately 10-fold. The increased uptake led to increased phototoxicity to MDA-MB-231 cells which well correlated with the increased cellular fluorescence signals. The increased photocytotoxicity was however better appreciated at the low $TPPS_4$ concentrations inducing death only in a fraction of cells. Both the remarkable fluorescence of $TPPS_4$ observed in cells as well as the extent of cell photoinactivation, cannot be ascribed to an internalization of the dcNPs without disassembling of the PDT agent. In fact, spectroscopic and photochemical results obtained in both aqueous solution and DMEM FBS+ showed negligible red fluorescence and barely detectable signal of the excited triplet state precursor of the $^1O_2$ as a result of the extensive aggregation of the PDT agent in the dcNPs, mainly as H-type aggregates, which are well known to be photochemically unactive.[35] As a consequence, we believe that $TPPS_4$ is most likely released as photoactive monomer, characterized by good fluorescence and excellent photodynamic properties, after cellular internalization.

The enhancement of DTX toxicity after incorporation into dcNPs was evident at the lowest tested concentration of 10 ng/mL. The higher cytotoxicity as compared to free DTX is very likely the consequence of a faster and more efficient block in the S and G2/M phases of the cell cycle. In fact, after 24 h of exposure, free DTX did not cause significant perturbations of the cell cycle while DXT-dcNPs caused an increase of the percentage of cells in S phase as well as G2/M. Slightly different are the effects described by Huang et al.[50] on the same cell line with 10 ng/mL DXT and this is very likely explained by the fact that cell cycle perturbations were analyzed after 48 h of treatment; in any case, in agreement with our observations, the arrest in G2/M phases was more evident with DTX-dcNPs rather than with free DTX. At concentrations higher than 10 ng/mL DXT-dcNPs caused an arrest of the cells in the G2/M phases stronger than that of free DTX but this effect did not translate into increased cell death also after prolonged treatment (48 and 72 h). The dark cytotoxicity of DTX-dcNPs toward MDA-MB231 cells was not affected significantly by the incorporation of $TPPS_4$. On the contrary following light activation of DTX/$TPPS_4$-dcNPs, cell death was increased tremendously and reached 100% at drug concentrations less than 0.2 μg/mL. Extremely important is the observation that the combination of the two drugs in their free form, especially at concentrations below 0.2 μg/mL, was much less powerful in inducing cell death than the combination delivered through dcNPs. Whether the enhancement of cytotoxicity is the result of a synergistic interaction of the two treatments will be determined with properly planned experiments and analyses of the data. In any case, the results reported here strongly indicate that dcNPs represent a very useful tool to potentiate the

cytotoxic effects of the combination $TPPS_4$ plus light and DTX. Very likely NPs favour the perfect timing and location of delivery of the two drugs to cell targets, namely microtubules. DTX is a well-known microtubule-stabilizing agent that interferes with mitosis and cell division and cause death of breast cancer cells through mitotic catastrophe.[51] Also light activated $TPPS_4$ exerts its cytotoxic effects by perturbing the assembling of the mitotic spindle and arresting the cells in mitosis.[52] It can therefore be hypothesized that the high efficiency of DTX/$TPPS_4$-dcNPs in inducing cell death is related to a concerted action of the co-delivered drugs on reorganization of microtubules that leads to arrest in mitosis followed by death for excessive damage to mitotic apparatus.

Conclusions

We have proposed a novel type of targeted dcNPs nanoparticles for the combined chemotherapy and photodynamic therapy of cancers overexpressing CD44 receptor. These dcNPs are achieved by taking advantage of electrostatic interactions between different building blocks, are decorated with HA as a targeting moiety, co-encapsulate the chemotherapeutic DTX and the PDT agent $TPPS_4$ in the core and the shell, respectively. dcNPs have the PDT agent completely aggregated and photochemically inactive at their surface and release it as active monomer after cell internalization. This feature is of relevance in view of further in vivo studies. Indeed, the dcNPs are expected to be non-fluorescent and non-photoactive while in the circulatory system. Targeting mechanisms localize the dcNPs in tumor tissue, where the PDT component is disassembled from the dcNPS surface and becomes highly fluorescent and phototoxic. The concerted release of the chemotherapeutic results in a tremendous improvement of single drug activity. This strategy turns to be very attractive to selectively co-localize different drugs in the same cell compartment and to find out possible synergic effects.

Acknowledgments

S. S. acknowledges the financial support of AIRC (IG2012-12834) and MIUR (PRIN 2011, 2010C4R8M8_004).

References

1 C. M. J. Hu, L. Zhang, *Biochemical Pharmacology* 2012, **83**, 1104.
2 M. F. Zuluaga, N. Lange, *Curr. Med. Chem.* 2008, **15**, 1655.
3 J. Lehar, A. S. Krueger, W. Avery, A. M. Heilbut, L. M. Johansen, E. R. Price, R. J. Rickles, G. F. Short, III, J. E. Staunton, X. Jin, M. S. Lee, G. R. Zimmermann, A. A. Borisy, *Nat. Biotechnol.* 2009, **27**, 659.
4 A. Khdair, D. Chen, Y. Patil, L. Ma, Q. P. Dou, M. P. Shekhar, J. Panyam, *J. Control Release* 2010, **141**, 137.
5 M. F. Zuluaga, N. Lange, *Curr. Med. Chem.* 2008, **15**, 1655.
6 P. Parhi, C. Mohanty, S. K. Sahoo, *Drug Discov. Today* 2012, **17**, 1044.
7 C. Conte, F. Ungaro, A. Mazzaglia, F. Quaglia, in *Nano-Oncologicals* (Eds: M. J. Alonso, M. Garcia-Fuentes), Springer International Publishing **2014**, 123.
8 P. Agostinis, K. Berg, K. A. Cengel, T. H. Foster, A. W. Girotti, S. O. Gollnick, S. M. Hahn, M. R. Hamblin, A. Juzeniene, D. Kessel, M. Korbelik, J. Moan, P. Mroz, D. Nowis, J. Piette, B. C. Wilson, J. Golab, *CA Cancer J. Clin.* 2011, **61**, 250.
9 P. Couvreur, *Advanced Drug Delivery Reviews* 2013, **65**, 21.
10 S. P. Egusquiaguirre, M. Igartua, R. M. Hernandez, J. L. Pedraz, *Clinical & Translational Oncology* 2012, **14**, 83.
11 C. M. Hu, R. H. Fang, B. T. Luk, L. Zhang, *Nanoscale.* 2014, **6**, 65.
12 K. K. Jain, *BMC. Med.* 2010, **8**, 83.
13 R. K. Jain, T. Stylianopoulos, *Nat. Rev. Clin. Oncol.* 2010, **7**, 653.
14 S. Nazir, T. Hussain, A. Ayub, U. Rashid, A. J. MacRobert, *Nanomedicine-Nanotechnology Biology and Medicine* 2014, **10**, 19.
15 N. Kamaly, Z. Y. Xiao, P. M. Valencia, A. F. Radovic-Moreno, O. C. Farokhzad, *Chem. Soc. Rev.* 2012, **41**, 2971.
16 J. Fang, H. Nakamura, H. Maeda, *Advanced Drug Delivery Reviews* 2011, **63**, 136.
17 H. Maeda, *Journal of Controlled Release* 2012, **164**, 138.
18 N. T. Huynh, E. Roger, N. Lautram, J. P. Benoit, C. Passirani, *Nanomedicine (Lond)* 2010, **5**, 1415.
19 N. Bertrand, J. Wu, X. Xu, N. Kamaly, O. C. Farokhzad, *Adv. Drug Deliv. Rev.* 2013.
20 E. Mahon, A. Salvati, F. Baldelli Bombelli, I. Lynch, K. A. Dawson, *Journal of Controlled Release* 2012, **161**, 164.
21 E. Pasquier, M. Kavallaris, N. Andre, *Nat Rev Clin Oncol* 2010, **7**, 455.
22 W. Fan, B. Shen, W. Bu, F. Chen, Q. He, K. Zhao, S. Zhang, L. Zhou, W. Peng, Q. Xiao, D. Ni, J. Liu, J. Shi, *Biomaterials* 2014, **35**, 8992.
23 G. H. Xiang, G. B. Hong, Y. Wang, D. Cheng, J. X. Zhou, X. T. Shuai, *Int. J. Nanomedicine.* 2013, **8**, 4613.
24 W. Miao, G. Shim, S. Lee, S. Lee, Y. S. Choe, Y. K. Oh, *Biomaterials* 2013, **34**, 3402.
25 C. Conte, F. Ungaro, G. Maglio, P. Tirino, G. Siracusano, M. T. Sciortino, N. Leone, G. Palma, A. Barbieri, C. Arra, A. Mazzaglia, F. Quaglia, *Journal of Controlled Release* 2013, **167**, 40.
26 D. Separovic, P. Breen, N. B. Boppana, B. E. Van, N. Joseph, J. M. Kraveka, M. Rahmaniyan, L. Li, T. I. Gudz, A. Bielawska, A. Bai, J. Bielawski, J. S. Pierce, M. Korbelik, *Int. J. Oncol.* 2013, **43**, 2064.
27 F. Danhier, E. Ansorena, J. M. Silva, R. Coco, A. Le Breton, V. Préat, *Journal of Controlled Release* 2012, **161**, 505.
28 D. A. Ossipov, *Expert Opin. Drug Deliv.* 2010, **7**, 681.
29 K. Y. Choi, G. Saravanakumar, J. H. Park, K. Park, *Colloids and Surfaces B-Biointerfaces* 2012, **99**, 82.
30 S. Misra, P. Heldin, V. C. Hascall, N. K. Karamanos, S. S. Skandalis, R. R. Markwald, S. Ghatak, *FEBS J.* 2011, **278**, 1429.
31 A. Almalik, S. Karimi, S. Ouasti, R. Donno, C. Wandrey, P. J. Day, N. Tirelli, *Biomaterials* 2013, **34**, 5369.
32 M. H. El-Dakdouki, X. Pure E FAU - Huang, X. Huang, *Nanoscale* 2013.
33 F. Ungaro, G. De Rosa, A. Miro, F. Quaglia, *Journal of Pharmaceutical and Biomedical Analysis* 2003, **31**, 143.
34 N. C. Maiti, S. Mazumdar, N. Periasamy, *Journal of Physical Chemistry B* 1998, **102**, 1528.
35 S. C. M. Gandini, V. E. Yushmanov, I. E. Borissevitch, M. Tabak, *Langmuir* 1999, **15**, 6233.
36 E. G. McRae, M. Kasha, *The Journal of Chemical Physics* 1958, **28**, 721.

37 R. Pandey, G. Zheng, *The Porphyrine Handbook*, Academic Press, San Diego **2000**.
38 D. K. Chatterjee, L. S. Fong, Y. Zhang, *Adv. Drug Deliv. Rev.* 2008, **60**, 1627.
39 K. Kalyanasundaram, M. Neumann-Spallart, *J. Phys. Chem.* 1982, **86**, 5163.
40 I. D'Angelo, C. Conte, A. Miro, F. Quaglia, F. Ungaro, *Expert Opinion on Drug Delivery* 2014, **11**, 283.
41 L. Mazzaferro, J. D. Breccia, M. M. Andersson, B. Hitzmann, R. Hatti-Kaul, *International Journal of Biological Macromolecules* 2010, **47**, 15.
42 C. D. Walkey, W. C. Chan, *Chem. Soc. Rev.* 2012, **41**, 2780.
43 A. Almalik, R. Donno, C. J. Cadman, F. Cellesi, P. J. Day, N. Tirelli, *Journal of Controlled Release* 2013, **172**, 1142.
44 S. Mizrahy, S. R. Raz, M. Hasgaard, H. Liu, N. Soffer-Tsur, K. Cohen, R. Dvash, D. Landsman-Milo, M. G. Bremer, S. M. Moghimi, D. Peer, *J. Control Release* 2011, **156**, 231.
45 F. Wilkinson, W. P. Helman, A. B. Ross, *Journal of Physical and Chemical Reference Data* 1993, **22**, 113.
46 J. Moan, Q. Peng, J. F. Evensen, K. Berg, A. Western, C. Rimington, *Photochemistry and Photobiology* 1987, **46**, 713.
47 J. F. Evensen, J. Moan, *Photochemistry and Photobiology* 1987, **46**, 859.
48 K. Berg, J. C. Bommer, J. W. Winkelman, J. Moan, *Photochemistry and Photobiology* 1990, **52**, 775.
49 G. Varchi, V. Benfenati, A. Pistone, M. Ballestri, G. Sotgiu, A. Guerrini, P. Dambruoso, A. Liscio, B. Ventura, *Photochemical & Photobiological Sciences* 2013, **12**, 760.
50 J. Huang, H. Zhang, Y. Yu, Y. Chen, D. Wang, G. Zhang, G. Zhou, J. Liu, Z. Sun, D. Sun, Y. Lu, Y. Zhong, *Biomaterials* 2014, **35**, 550.
51 D. L. Morse, H. Gray, C. M. Payne, R. J. Gillies, *Molecular Cancer Therapeutics* 2005, **4**, 1495.
52 K. Berg, J. Moan, J. C. Bommer, J. W. Winkelman, *International Journal of Radiation Biology* 1990, **58**, 475.